STUDIA UBB CHEMIA, LXVII, 4, 2022 (p. 151-167)
(RECOMMENDED CITATION)
DOI:10.24193/subbchem.2022.4.10

# INVESTIGATION OF THE FUNCTIONAL LAYER FORMATION ON THE SURFACE OF CARBON MATERIAL

**Saken ABDIMOMYN[a], Azhar ATCHABAROVA[a,*], Dinara ABDUAKHYTOVA[a], Rustam TOKPAYEV[a], Kanagat KISHIBAYEV[a], Tamina KHAVAZA[a], Andrey KURBATOV[a], Graziella Liana TURDEAN[b], Mikhail NAURYZBAYEV[a]**

**ABSTRACT.** In this study, a comparison of walnut-based carbon materials (CM) obtained by hydrothermal carbonization (HTC) and HTC in combination with steam gas activation (SGA) was carried out. In order to study the effect of steam activation on the functional layer formation, the obtained materials were studied by SEM, nitrogen adsorption/desorption by Brunauer-Emmett-Teller (BET) method, Raman spectroscopy, X-ray diffraction spectroscopy (XRD), X-ray fluorescence elemental analysis (XRF). Functional groups (FG) were evaluated qualitatively and quantitatively by Fourier transform infrared spectroscopy (FTIR), acetone extract analysis of CM by gas chromatography-mass spectrometry (GC-MS), and potentiometrically Boehm titration. The described mechanism of the influence of the base nature on the surface functionality correlates well with the results of the powder addition method. The HTC or HTC+SGA treatment provides a wide range of possibilities for further controlled modification of the carbon sorbent surface for specific adsorption purposes.

***Keywords:*** *hydrothermal carbonization, carbon material, thermal carbonization, walnut shell, activated carbon, functional layer.*

## INTRODUCTION

Our days, the pollution of water resources with heavy metals (HM) and organic compounds (OC) is a great challenge that must be solved to assuring a high-quality lifestyle [1,2]. In this context, carbon materials are

[a] *Center of Physical Chemical Methods of Research and Analysis, al-Farabi Kazakh National University, Almaty, Kazakhstan*
[b] *Babeş-Bolyai University, Faculty of Chemistry and Chemical Engineering, 11 Arany Janos str., RO-400028, Cluj-Napoca, Romania*
* *Corresponding author: atchabarova.azhar@kaznu.kz*

©2022 STUDIA UBB CHEMIA. Published by Babeş-Bolyai University.

This work is licensed under a Creative Commons Attribution-NonCommercial-NoDerivatives 4.0 International License.

promising compounds as adsorbents because of their low cost, high specific surface area, chemical inertness, and a great variety of surface functional groups [3-5]. Also, a chemical modification of CM has beneficial effects and is a widely used method to improve the adsorption properties and electrochemical characteristics of CM by increasing the specific surface area of the sample and forming a functional layer on the activated carbon surface.

Usually, chemical modification occurs by $CO_2$, $H_2O_{vapor}$, NaOH, KOH, $ZnCl_2$, $FeCl_3$, $K_2CO_3$, $H_2SO_4$, $H_3PO_4$, and $HNO_3$ treatment [9, 10]), but an electrochemical modification [6] could be also performed.

In function of the applied chemical modification procedure the following properties can be modified (i) specific surface area ($S_{specific}$) (*e.g.,* see the study of macadamia nutshells, corn cobs, and rice husks activated with either $CO_2$ or $H_2O_{vapor}$ [8]), (ii) a decrease of the volume of mesopores, the degradation of the carbon skeleton, the narrowing of pores if the activation treatment with KOH and NaOH occurs at prolonged high temperatures [7], (iii) partial destruction of the carbon structure, breaking of carbon-carbon bonds, and addition of oxygen leading to the formation of carboxylic, anhydride, carbonyl, lactone, phenolic, ketone, lactone, and ether groups on the activated carbon surface after treatment with $HNO_3$ of the porous carbon material [11]. It should be noticed, that in these cases, the pore size distribution and surface area are determined by the ratio between the chemical activator and the carbon raw material [12].

Either chemical modification or electrochemical modification of CM leads to an increase in selectivity and adsorption capacity of heavy metals ions and organic compounds and consequently to their use as sensing interfaces for catecholamines [13], glucose [14], dopamine, adrenaline, uric acid [15, 16], $Cu^{2+}$, $Ni^{2+}$, and $Pb^{2+}$ [17-19] determination.

It is worth mentioning that last years, much attention is paid to the development of sorbents and enterosorbents based on components of plant origin and living organisms. Adsorbents of this type are the following: alginates [20], pectins [21], and chitin [22]. However, the technologies for obtaining such polysaccharides are relatively high energy- and time-consuming. In addition, enterosorbents have rather low mechanical strength and relatively high cost, which limits their widespread use. Consequently, agricultural wastes (walnut shells, grape and apricot seeds, spruce and pinecones, etc.) are the most promising raw materials for activated carbon materials (ACM) preparation [23].

This work aims to study the carbon materials (CM) based on walnut shells and the effect of vapor-gas activation on the formation of a functional layer on the surface of the activated carbon (AC). The morpho-structural features of the AC were obtained by BET, SEM, XRD, XRF, Raman spectroscopy investigations.

Also, FTIR, Boehm's titration, GC-MS methods were used to explain the mechanism of interaction of aqueous solution components with the surface of the AC.

## RESULTS AND DISCUSSION

### *Study of the basic physico-chemical characteristics of the AC samples*

The use of porous structures with high specific surface area and different pore size distribution is of key importance for the high capacity of the materials in adsorption and electrochemical processes.

The results of $N_2$ adsorption-desorption analysis by the BET method and the pore distribution are presented in Table 1 and Figures 1. The treatment of CM with acute water vapor opens the micropores, which leads to an increase of $S_{specific}$, evidenced by the increase in the average size of micropores from 1.24 nm to 1.74 nm, and the corresponding decrease of the percentage of microporosity from 87.5 and 84.09 %, respectively.

**Table 1.** Results on the specific surface area and porosity of activated carbons based on plant waste

| Activated carbon | $S_{specific}$ / $m^2 \cdot g^{-1}$ | $V_{total}$ / $cm^3 \cdot g^{-1}$ | $V_{mN2}$ / $cm^3 \cdot g^{-1}$ | % of micropores | Micropore volume till 2 nm from $N_2$ / $cm^3 \cdot g^{-1}$ | Average pore width / nm | Adsorption enegy (Dubinin-Radushkyevich method) / kJ $mol^{-1}$ |
|---|---|---|---|---|---|---|---|
| **HTC** | 464.9 | 0.24 | 0.21 | 87.50 | 0.20 | 1.24 | 20.86 |
| **HTC+SGA** | 738.0 | 0.22 | 0.19 | 84.09 | 0.16 | 1.74 | 14.92 |

The obtained BET results demonstrate that the ACM samples before and after activation retain a microporous structure up to 2 nm (Figures 1 inset).

It can be concluded that the presence of pores no larger than 4 nm in the ACM sample after HTC indicates an activated carbon mesoporous structure which allows the hydrated ions to penetrate freely into the structure of the material. However, as can be seen from Figure 1, the disappearance of the pores greater than 4 nm width and the increase of the intensity of pores with 2 nm width after activation is probably due to the release of non-carbon components, such as oxygen and nitrogen, during the activation process. This leads to the formation of a large distribution of micropores in the sample structure.

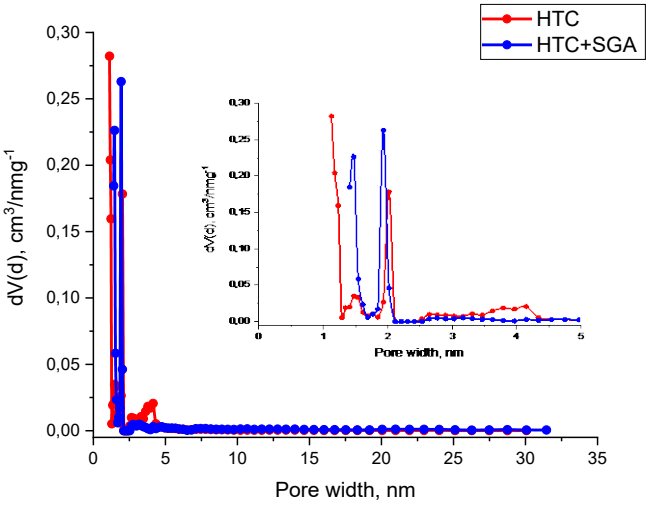


**Figure 1.** Pore size distributions of CM activated by HTC and HTC+SGA.

The adsorption isotherm for the ACM samples after hydrothermal carbonization (Figure 2, red line) is described by the Freundlich isotherm. According to this, there are adsorption sites with high and low affinity to the adsorbate on the heterogeneous surface. The high-affinity sites are engaged first, which explains the sharp increase at low pressure. Another reason is probably the lateral repulsion between the adsorbed molecules [24].

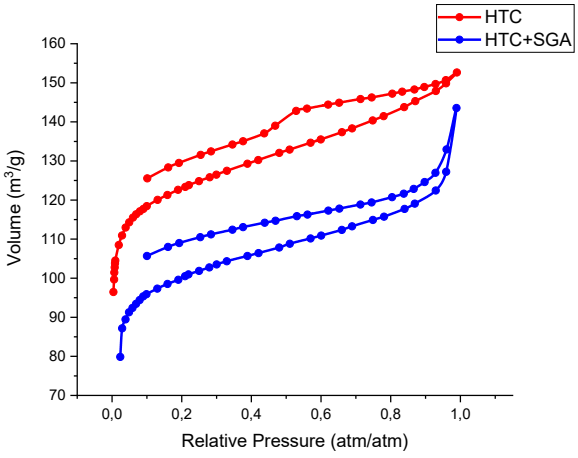


**Figure 2.** Nitrogen adsorption-desorption isotherms of CM activated by HTC (red line) and HTC+SGA (blue line).

The results of nitrogen adsorption isotherms indicate that steam gas activation of carbon increases the number of adsorption sites, which leads to the hypothesis of additional layer formation, due to the destruction of non-carbon components of the matrix and the chemical conversion of water from the surface.

To confirm the hypothesis of an increase in $S_{specific}$ due to matrix destruction, a micrograph of the sample surface was performed. The microphotographs of CM after HTC and HTC+SGA activation are presented in Figures 3. The surface of powders is shown as textural rough, with pores of different sizes distributed randomly. It can be concluded that steam gas activation of AC samples leads to an increase in surface area, due to the penetration of water vapor in pores. The formation of porous and defective carbon structure can be explained by the release of non-carbon elements such as $H_2$, $O_2$, and $N_2$ from the carbonizat's surface during the pyrolysis process, with the formation of a rigid carbon skeleton having a rudimentary porous structure. The structure of the samples after SGA is represented by flaky and round rod-like structures aggregated into larger particles.

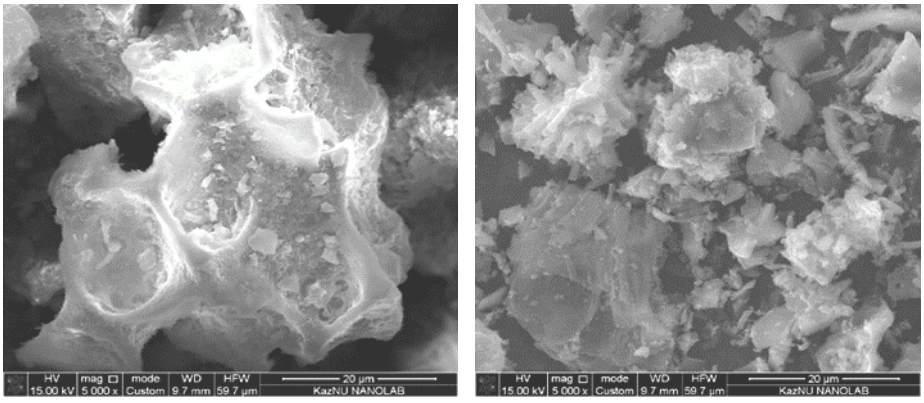


**Figure 3.** Surface morphology of CM samples based on walnut shells activated by HTC (A) and HTC+SGA (B)

According to the XRF analysis results (Table 2), ACM based on walnut shells contains significant amounts of K and Ca and trace amounts of other elements. The accumulation of K and Ca by plants and the subsequent formation of complexes and compounds based on covalent bonds leads to the finding of residual elements in the structure of the carbon matrix either after carbonization or after the activation treatment. It is assumed that after activation, the content of elements decreases due to the diffusion of ions into the aqueous component of the mixture.

**Table 2.** Results of elemental analysis by XRF of ACM based on plant waste

| | Concentration of elements / % | | | | | | | | | | |
|---|---|---|---|---|---|---|---|---|---|---|---|
| | Mg | Si | P | S | Cl | K | Mn | Fe | Cu | Zn | Ca |
| **HTC** | 0.16 | 0.48 | 0.11 | 0.05 | 0.04 | 2.32 | 0.04 | 4.54 | 0.03 | 0.03 | 7.21 |
| **HTC+SGA** | 0.00 | 0.22 | 0.06 | 0.03 | 0.02 | 1.32 | 0.01 | 0.59 | 0.03 | 0.02 | 1.89 |

The effect of steam-gas activation on the crystal structure formation was evaluated by Raman spectroscopy (Figure 4, Table 3) and XRD methods (Figure 5).

The Raman spectrum of the CM sample activated by HTC+SGA (Figure 4) is characterized by two characteristic bands which are observed in the regions of 1580, and 1600 cm-1 and which correspond to the undisturbed graphite lattice where the ideal modes of the vibrations of graphite lattice have E2g symmetry. At 1620 $cm^{-1}$ is the characteristic graphite scattering peak and the first order $D_2$ band.

The spectrum of the sample HTC+SGA shows additional first-order bands (D bands or defect bands), which are characteristic of disordered graphite. Its intensity increases in comparison with the G band as the degree of disorder in the graphite structure increases. The most intense of them is the $D_1$ band, which appears at 1360 $cm^{-1}$ and corresponds to the graphite lattice vibration mode with $A_{1g}$ symmetry [7].

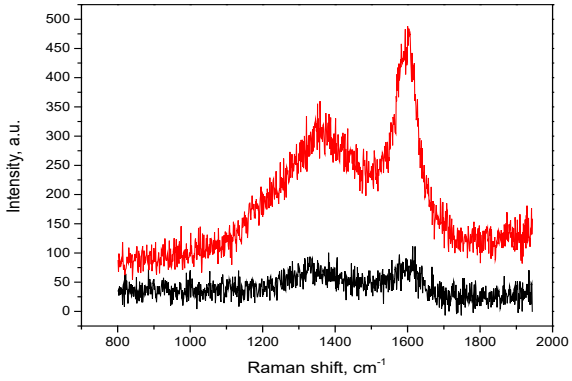


**Figure 4.** Raman spectra of CM based on walnut shells activated by HTC (black line), HTC+SGA (red line)

**Table 3.** $I_G/I_D$ ratio value and $L_a$ calculation for activated carbons

| | **$I_D/I_G$ ratio** | **$L_a$ / nm** |
|---|---|---|
| **HTC** | 0.85 | 4.98 |
| **HTC + SGA** | 0.67 | 6.67 |

It was found that the $I_D/I_G$ ratio decreased after activation with water vapor, which indicates an increase in the crystallinity of the sample (Table 3). The phenomenon confirms the combustion of non-carbon components, while the carbon skeleton remains. A correlation between the $I_D/I_G$ ratio and the crystallite size ($L_a$) is observed. This behavior is a consequence of burning out the amorphous structure of carbon. The crystallinity of the samples demonstrated by Raman investigation was estimated by peak integration. It was equal to 94.19 and 70.81% for HTC and HTC+SGA activation, respectively [26].

The diffractograms of CM activated by HTC and HTC+SGA (Figure 5) showed wide peaks at 2Ɵ ~ 20 - 28° and 44°, which are characteristic peaks of raw material based on the plant. The presence of peaks at 2Ɵ ~ 20 - 28° is confirmed by the amorphous structure of the obtained CM, which is due to the nature of the lattice plane structure (002) of the graphite carbon black.

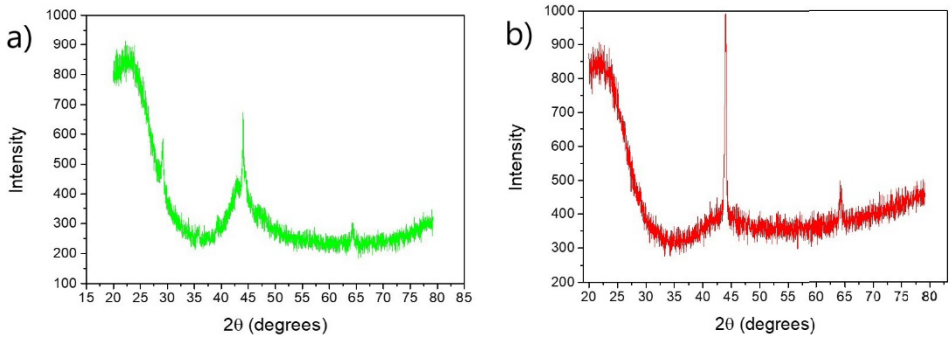


**Figure 5.** XRD spectra of CM activated by HTC (A) and HTC+SGA (B).

### *Determination of functional groups on the carbon samples surface*

It is necessary to qualitatively and quantitatively determine the hydrophilicity and hydrophobicity of carbon materials which are due to the distribution and concentration of surface functional groups to further optimize the process of chemical and electrochemical modification by selecting modifiers, solution pH, electrolyte composition, electrolyte activity, and electrochemical modification methods.

Qualitative and quantitative determination of functional groups present on the carbon materials surface was carried out using infrared spectroscopy, GC-MS, and potentiometric Boehm titration methods.

By FTIR investigation (Figures 6), it was found that the samples based on the walnut shell are characterized by the presence of conjugated -C=C-, aromatic ring, and Ph- in the interval $v$ = 1599-1605 $cm^{-1}$; Ar-OH- at $v$ = 1359.98; -$CH_2$-CO-, -OH, -CN- at $v$ = 1398-1401 $cm^{-1}$; Alk-O-$CH_3$, Ar-O-$CH_3$ at $v$ = 2831.85 $cm^{-1}$; -NH-SO-, -$CH_2$-SOH, -$CH_2$-CO-$CH_2$ at $v$ = 1701 $cm^{-1}$; and the presence of intermolecular hydrogen bonds between $v$ = 3404-3408 $cm^{-1}$. However, the intensities of the above bands increase for ACM by HTC + SGA. In addition, steam-gas activation of carbon promotes the formation of functional groups -OH at $v$ = 3.745 $cm^{-1}$, -NH-SO-, -$CH_2$-COH-, -$CH_2$-CO-$CH_2$ at $v$ = 1701 $cm^{-1}$, which indicates the formation of the functional layer on its surface.

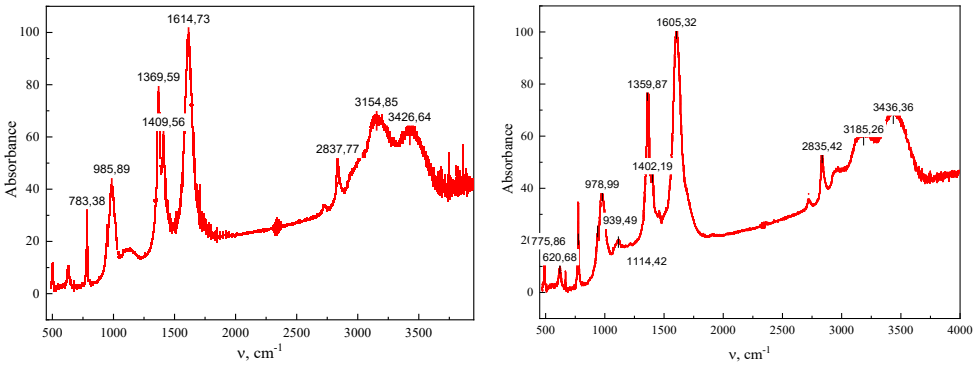


**Figure 6.** FTIR spectrum of the walnut shell sample activated by HTC (A) and HTC+SGA (B).

According to a literature review, the following functional groups could be formed on the surface of the carbon material activated by steam gas activation [27]. Thus, carboxyl surface groups (R-COO-, have characteristic acidic hydrolysis in aqueous solutions and can form anhydrides if they are close to the basal planes of carbon), single hydroxyl groups (-OH, at the edge of the "aromatic" layers will be phenolic in nature), carbonyl groups (C=O, obtained by the formation of lactones or simple ester groups from adjacent carboxyl and hydroxyl groups) are identified [28]. In our case, the GC-MS analysis of the samples extracted in acetone shows the presence of polar substances with the previously mentioned functional groups: -C=O, -COOH, -OH, -C-O-C-, aryl- and alkyl derivatives, -C(O)-NH-R, etc. The formation of polar functional groups on the functional layer of ACM is probably due (i) to the chemical interaction of CM with acute water vapor, or (ii) to the chemical adsorption of water molecules on the CM surface. The GC-MS results are in correlation with the information obtained from the IR spectra.

The qualitative determination of surface FG on carbon material is insufficient for further prediction of material behavior under conditions of chemical and electrochemical modification. For this reason, the potentiometric Boehm titration method was performed. As seen in Table 4, the distribution of functional group concentrations of different natures, expressed by mols per 1 gram or 1 $m^2$ of the CM surface, was calculated.

**Table 4.** The concentration of functional groups on the CM surface (HTC + SGA)

| | $C_i * 10^3$, mol/g | | | $C_i *10^6$, mol/$m^2$ | | |
|---|---|---|---|---|---|---|
| | C-OH | C=O | -COOH | C-OH | C=O | -COOH |
| **HTC+SGA** | 1.15 | 0.87 | 6.31 | 1.53 | 1.15 | 8.37 |

According to Boehm's method the phenolic, lactone, and carboxyl functional groups follow a neutralization reaction with 0.1 M solutions of bases of different strengths: NaOH, $Na_2CO_3$, and $NaHCO_3$, respectively. The mechanism of the neutralization reaction between the surface organic FG and 0.1 M of different base solutions is described below.

A differential potentiometric titration curve when adding $NaHCO_3$ is presented in Figure 7B. The presence of 2 peaks is due to the acid-base interaction of the following proposed mechanism (reaction 1):

$$R\text{-}COOH + NaHCO_3 = R\text{-}COONa + CO_2 + H_2O,\ pH = 4 - 5$$

where: R is in the carbon matrix of the sorbent.

**Scheme 1**

As known, the weak base $NaHCO_3$ has a good affinity to the carboxyl group, allowing the reaction (Scheme1) to occur at the carbon FG group - solution interface. It is possible to assume the equality of the concentrations of carboxyl groups to the average value of $N(NaHCO_3)$ (reaction 2) [29].

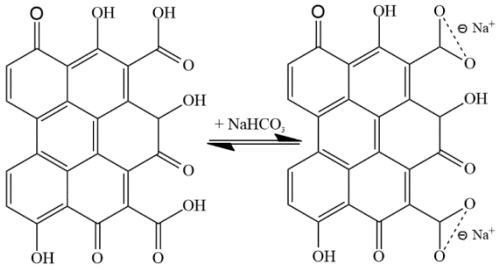


**Scheme 2**

However, when 0.1 M NaOH is added to activated carbon (Figure 7A), an ionization of almost all FGs from the surface of the carbon matrix occurs, which is visible on the differential potentiometric titration curve by a single peak.

According to the literature review, the $pK_a$ values of their conjugated acids varied from 6 - 8. They form oxonium ions with strong protonic acids, that subsequently are stabilized by resonance structures presented in scheme 3 [30]:

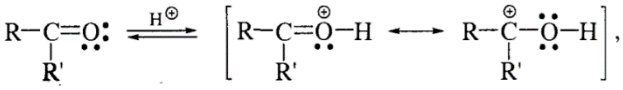

**Scheme 3**

Also, when the strong base NaOH is added, hydration of the surface aldehyde group occurs due to the high nucleophilicity of the hydroxide ion. For this reason, the hydroxide ion quickly attacks the positively charged carbon by the following mechanism (Scheme 4) [31]:

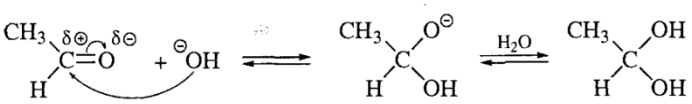

**Scheme 4**

As a result, the addition of a strong protonic acid leads to the formation of hydroxyl groups, which are neutralized by NaOH (reaction 5).

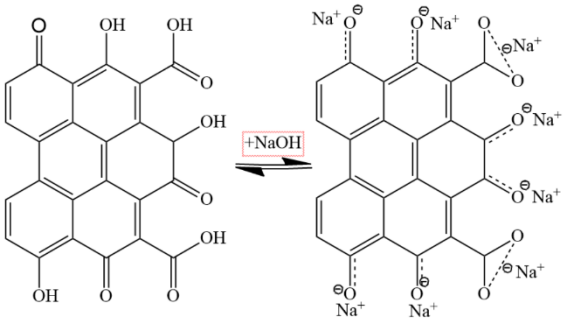


**Scheme 5**

Functional groups (having $pK_a$ in the range of 4 - 10) as carboxyl, lactone, and carbonyl groups are neutralized following the reaction (6), when $Na_2CO_3$ is added (Figure 7C). In this case, hydroxyl groups are not affected due to their high hydration energy.

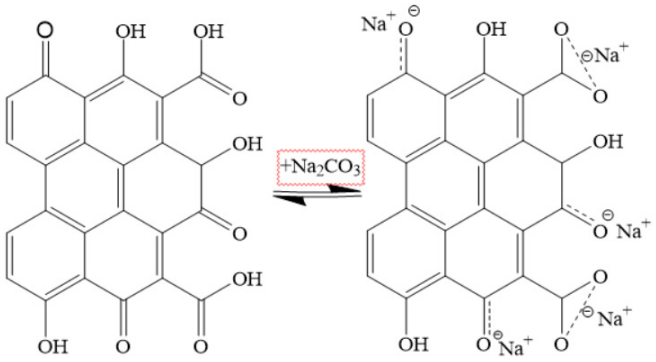


**Scheme 6**

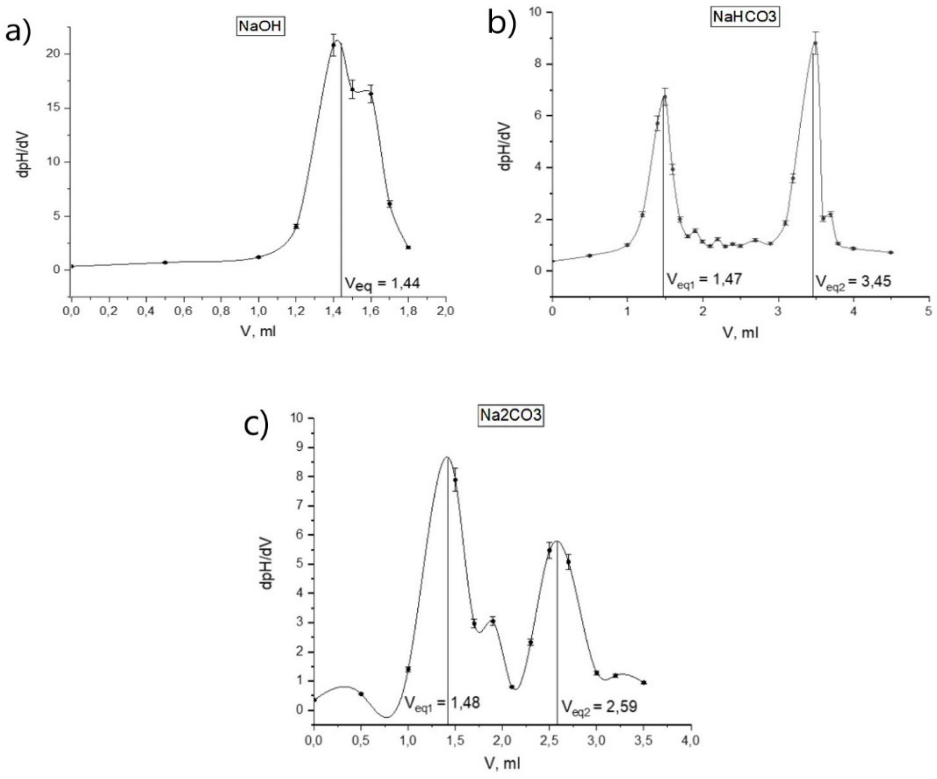


**Figure 7.** First derivative of the titration curves for direct titration of the functional groups of ACM with 0.1 M solutions of NaOH (A), $NaHCO_3$ (B), $Na_2CO_3$ (C).

***Powder addition method***

Using the powder addition method, the pH point of zero charge ($pH_{pzc}$) of CM activated by HTC+SGA in 0.01 M solutions of $Na_2SO_4$ and $K_2SO_4$ were determined. Thus, the pH of the solutions was measured after 24 hours that CM powders were mixed with $Na_2SO_4$ or $K_2SO_4$ (Figure 8). With both used solvents, the carbon material exhibits basic surface properties due to the presence of surface oxygen-containing groups. A plateau is observed on the graph at $pH_i$ = 4-5, which indicates that the carboxyl and carbonyl surface groups are in molecular form. However, it should be noted that the hydroxyl groups are also in the molecular form due to the $pK_a$ = 9 - 10. There is a correlation between $pH_f$ - $pH_i$ *versus* $pH_i$ in the pH = 4-5 range, which suggests that the $pK_a$ values of the carboxyl and carbonyl groups are placed between 4-6 [32].

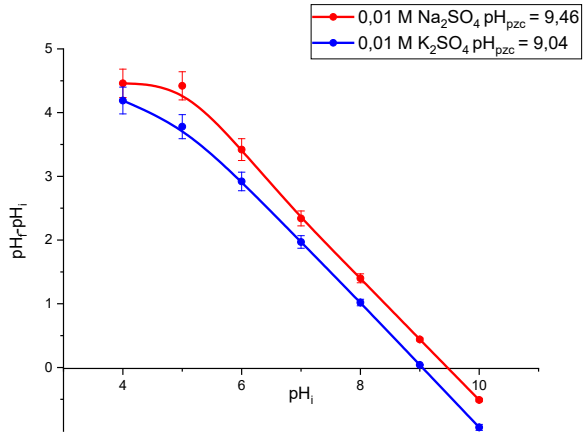


**Figure 8.** The $pH_{zpc}$ determination for CM activated by HTC+SGA estimated in 0.01 M $Na_2SO_4$ (red line), 0.01 M $K_2SO_4$ (blue line).

The linear decrease of the values of $pH_f$ - $pH_i$ difference is observed in the pH = 5-9 range and is a consequence of carboxyl groups ionization, and carbonyl groups dissociation on CM surface. Consequently, the assumed mechanism of groups dissociation and ionization follows the reactions 7:

$$\begin{aligned} R\text{-}COOH &= R\text{-}COO^- + H^+ \\ R\text{-}C{=}O + e &= R\text{-}CO^- \end{aligned} \qquad (7)$$

The complete dissociation of the -OH groups from the surface, following reaction 8, corresponding to $pH_i$ = 9 - 9.5, is attributed to quinone and phenolic groups on the surface. [33].

$$R\text{-}OH = R\text{-}O^- + H^+ \quad (8)$$

It must be noticed that the difference in $pH_f$ - $pH_i$ values depend on the nature of the cation, being with 0.5 pH units higher in the case of $Na^+$ than for $K^+$, respectively. This is probably due to less hydration of the $K^+$ cation which promotes either its penetration into the pores of the carbon sorbent or the establishment of a rapid equilibrium at the carbon-solution phase boundary [34]. A consequence of this assumption is the consideration of the series $H^+ < Li^+ < Na^+ < K^+$, where the hydration energy decreases from right to left according to the electrostatic theory of solvation. Therefore, the $Na^+$ ion has the most pronounced acidic properties compared to the $K^+$ ion [35].

From the results of the powder addition method, it can be concluded that the formation of the oxygen-containing functional layer (OFL) on the surface is caused by the degree of oxidation of carbon material and the nature of the modifier, and can allow acid-base interactions on the surface of the carbon material. It can be assumed that the material surface is partially protonated and undissociated at pH < 5, and the carbon matrix removes anionic particles from the diffusion region of the electrical double layer. But at pH > 5, the surface partially acquires a negative charge due to the dissociation of carboxyl and carbonyl groups. It is noticeable that the dissociation of hydroxyl groups gives an additional negative charge to the surface, at pH > 9.

Thus, the formation of acid-base centers on the surface of the activated carbon material opens the possibility for different applications like the specific adsorption of heavy metals from aqueous solutions [17].

## CONCLUSION

Activated carbon materials having sorbents properties, based on walnut shells were obtained by hydrothermal carbonization with steam gas activation method (*i.e.*, HTC and HTC+SGA), respectively. Steam gas activation was carried out to increase the porosity and to form a functional layer on the surface on the material. BET results and pore size distribution revealed that the activation of the carbon sorbent leads to a 2-fold increase in the surface area compared with the walnut shell carbonizate. It indicates the opening of micropores and their increase due to carbon oxidation ($S_{specific}$ = 464.9 $m^2/g$ for the CM activated by HTC, $S_{specific}$ = 738.0 $m^2/g$ for the CM activated by HTC+SGA). Oxygen-containing functional groups on the surface were qualitatively determined by both FTIR and GC-MS measurements. The functional groups -OH, -C=O, and -COOH were quantified by potentiometric Boehm titration method. The supposed mechanism of the neutralization of

the functional groups depending on the nature of the used base is described. The powder addition method for $pH_{pzc}$ determination confirms the presence of oxygen-containing FG and the results are in good correlation with those obtained by titration, FTIR, and GC-MS.

Thus, the activated carbon sorbent is characterized by acid-base centers, which open the way to possible modifications of the surface for specific adsorption of heavy metals and organic substances from aqueous solutions with modern applications.

## EXPERIMENTAL SECTION

### *Reagents and equipment*

The following reagents were used in this work: KBr, $K_2SO_4$, $Na_2SO_4$, acetone, $H_2SO_4$ (from Sigma Aldrich), ethyl alcohol, (99%); ultra-high dispersion polyethylene powder (UHPP, from GUR®, USA), argon, (from Sigma Aldrich). All chemicals were of chem purity.

### *Methodology of carbon materials obtaining*

Carbon materials (CM) based on walnut shells were obtained by hydrothermal carbonization at T = 240 $^0$C for 24 hours (HTC) in a steel autoclave reactor. The ratio of the material to water was 1: 2. In order to increase the specific surface of CM and the formation of oxygen-containing functional groups on the surface, the material was activated by acute water vapor at T = 800-850 $^0$C for 60-70 minutes (HTC+SGA). Further, the sorbent was crushed to a fraction of 56 μm on a planetary monomill (model PULVERISETTE 6, from Fritsch, Russia) [23, 25].

### *Methods of carbon sorbents studying*

The nitrogen adsorption/desorption method was used to evaluate the carbon sorbents' morphological features. $S_{specific}$ and adsorption isotherms were obtained according to the BET polymolecular adsorption model. The total pore volume ($V_{tot}$) and micropore volume ($V_{micro}$) were calculated using density functional theory (DFT).

The SEM was used to evaluate the surface morphology of the samples using a field emission scanning electron microscope (model FE-SEM, equipped with an ultra-high resolution field emission scanning electron microscope, type Hitachi SU8020, Japan). The content of carbon sorbents mineral impurities was determined by X-ray fluorescence spectroscopy (EDXRF, using energy dispersive X-ray fluorescence spectrophotometer, type Epsilon 3 PANalytical B, from Malvern Panalytical, United Kingdom), X-ray diffraction

(XRD, using a X-ray diffractometer, type PANalytical, Philips, from Malvern Panalytical, United Kingdom, with Cu, Ka radiation, λ - 1.5418 Å), and Raman spectroscopy methods (using inVia™ confocal Raman microscope from Renishaw, United Kingdom) were used to characterize different allotropic modifications of carbon in the sample structure.

### *Methods the surface charge and surface functional groups determination of the carbon sorbents*

The FTIR measurements using a spectrometer (model FSM-1201, from LightMachinery, Canada) were performed to qualitatively evaluate the functionality of carbon sorbents in the interval of wave number $v$ = 4000-500 $cm^1$. The mass ratio of KBr:CM was 700:1.

The CM extract in acetone was prepared to qualitatively determination of the polar functional groups. A quantity of 0.5 g ACM was added to 5 ml of acetone and was ultrasounded for 60 minutes. Then, the obtained suspension was filtered using a 0.5 μm pore size membrane filter. The acetone extract was analyzed on a GC-MS (model 7890B GC & 5977A MSD, Agilent, USA).

The potentiometric Boehm titration method determined the nature and the quantitative content of oxygen-containing functional groups (OFG). For a better wettability of the ACM with basic solutions, the sample was prepared as follows. A quantity of 1.000 ± 0.001 gr of ACM mixed with 25.0 $cm^3$ of bidistilled water was degassed under ultrasound for 10 minutes; then 0.1 mol/L of NaOH solution was added to flasks, pumped out with air, and left for 3 days. The solutions were filtered, and 5 $cm^3$ of 0.1 mol/L HCl was added. The titration was done with a freshly prepared 0.1 mol/L NaOH solution and the equivalence point was estimated by potentiometry. Titration was carried out with a potentiometric automatic titrator (model ATP-02) equipped with a glass electrode.

The amount of NaOH used to neutralize the functional groups ($N_i$) was calculated according to the literature [36].

According to the stoichiometry, the neutralization reaction C(-COOH) is equal to the average value of $N(NaHCO_3)$; $C(-C=O) = N(Na_2CO_3) – N(NaHCO_3)$; $C(-OH) = N(NaOH) - N(Na_2CO_3)$.

The method of powder addition was used to determine the pH at which the surface charge of the activated carbon (ACM) is zero. A 0.01 M $Na_2SO_4$ and 0.01 M $K_2SO_4$ were used as electrolytes. They do not exhibit specific adsorption on the ACM. Adjustment of pH between 4 - 10 was performed using NaOH, KOH, and $H_2SO_4$ solutions without $CO_2$. The initial pH of the solution ($pH_i$) was recorded, and a certain amount of ACM (~5 g/L) was added to each test tube and filled with Ar. The final $pH_f$ value was measured after 24 hours of stirring on a shaker. The $pH_{pzc}$ was calculated as the extrapolation to $pH_f - pH_i = 0$ from the $pH_f - pH_i = f(pH_i)$ plot.

**ACKNOWLEDGEMENT**

This research was funded by the Science Committee of the Ministry of Education and Science of the Republic of Kazakhstan (Grant No. AP09058570).

## REFERENCES

1 A.G.B. Pereira, F.H.A. Rodrigues, A.T. Paulino, A.F. Martins, A.R. Fajardo; *J. Clean. Prod*., **2021**, *284*, 124703.
2 Ch. Su, Y. Guo, L. Yu, J. Zou, Z. Zeng, L. Li; *Mat. Chem. and Phys*., **2021**, *258*, 123930.
3 E. Frackowiak, B. Francois; *Carbon*, **2001**, *39*, 937-950. 4
4 M.A. Islam, S. Sabar, A. Benhouria, W.A. Khanday, M. Asif, B.H. Hameed; *J. Taiwan Inst. Chem. Engrs.,* **2017**, 74, 96-104.
5 J.L. Figueiredo; *J. Mater. Chem.*, **2013**, 1, 9351-9364.
6 P. González-García; *Renew. Sust. Energ. Rev*., **2018**, 82, 1393-1414.
7 S. Roldán, I. Villar, V. Ruíz, C. Blanco, M. Granda, R. Menéndez, R. Santamaría; *Energy Fuels*, **2010**, 24, 3422-3428.
8 A. Aworn, P. Thiravetyan, W. Nakbanpote; *J. Anal. Appl. Pyrolysis*, **2008**, 82, 279-285.
9 S.K. Theydan, M.J. Ahmed; *Powd. Tech*., **2012**, 224,101–108.
10 Y.A. Rahim, S.N. Aqmar, D.R. Dewi; *Mater. Sci. Eng*., **2012**, 4, 22-26.
11 C. Yang, Q. Pan, Q. Jia, Y. Xin, W. Qi, H. Wei, S. Yang, B. Cao; *Appl. Surf. Sci.*, **2020**, 502, 144-423.
12 Y. Nagakawa, M. Molina-Sabio, F. Rodríguez-Reinoso; *Micropor. Mesopor. Mater.*, **2007**, 103, 29-34.
13 G. Cui, J.H. Yoo, J.S. Lee, J. Yoo, J.H. Uhm, G.S. Cha, H. Nam; *Analyst,* **2001**, 126, 1399-1403.
14 K. Pliuta, A. Chebotarev, A. Koicheva, K. Bevziuk, D. Snigur; *Anal. Methods*, **2018**, 10, 1472-1479.
15 M. Velmurugan, N. Karikalan, S.M. Chen, Y.H. Cheng, C. Karuppiah; *J. Colloid Interface Sci.*, **2017**, 500, 54-62.
16 H.L. Chiang, C.P. Huang, P.C. Chiang; *Chemosphere*, **2002**, 47, 257-265.
17 J.R. Rangel-Mendez, M. Streat; *Water Res*., **2002**, 36, 1244-1252.
18 T. Van Tran, Q.T.P. Bui, T.D. Nguyen, N.T.H. Le, L.G. Bach; *Adsorpt. Sci. Technol.*, **2017**, 35, 72-85.
19 G. Yang, H. Chen, H. Qin, Y. Feng; *Appl. Surf. Sci.*, **2014**, 293, 299-305.
20 Z. Wang, Y. Huang, M. Wang, G. Wu, T. Geng, Y. Zhao, A. Wu; *J. Environ. Chem. Eng.,* **2016**, 4, 3185-3192.
21 S. Schiewer, S.B. Patil; *Bioresour. Technol.*, **2008**, 99, 1896-1903.
22 W. Boulaiche, B. Hamdi, M. Trari; *Appl. Water Sci*., **2019**, 9, 1-10.

23 A.A. Atchabarova, R.R. Tokpayev, A.T. Kabulov, S.V. Nechipurenko, R.A. Nurmanova, S.A. Yefremov, M.K. Nauryzbayev; *Eurasian Chem.-Technol. J.*, **2016**, 18, 141-147.
24 Arthur W. Adamson; "Physical Chemistry of Surfaces", Arthur W. Adamson, Alice P. Gast; A Wiley-Interscience publication, **1997**, 808 p.
25 A. Atchabarova, R. Tokpayev, A. Kabulov, S. Nechipurenko, S. Yefremov, M. Nauryzbayev; *Bull. of Univ. of Karaganda-Chem*., **2016**, 83, 66-71.
26 J. Serafin, M. Ouzzine, O.F. Cruz Junior, J. Sreńscek-Nazzal; *Biomass Bioenergy*, **2021**, 144, 105925.
27 H.P. Boehm; *Carbon*, **1994**, 32, 759-769.
28 X. Fan, Y. Lu, H. Xu, X. Kong, J. Wang; *J. Mater. Chem.*, **2011**, 21, 18753-18760.
29 D.S. Dmitriev, M.V. Ivakhiv, D.V. Agafonov; *Bull. of the St. Petersburg State Inst. of Techn.*, **2018**, 44, 21-25.
30 V.F. Traven; "Organic chemistry", *Academic Book*, Moscow, **2004**, 727 p.
31 I.D. Harry, B. Saha, I.W.; *J. Colloid Interface Sci.*, **2006**, 304, 9-20.
32 R.C. Bansal, J.-B. Donnet; "Surface Groups on Carbon Blacks", in *Carbon Black*, J.-B. Donnet, R.C. Bansal, M.-J. Wang Eds.; Routledge, New York, **1993**, 46 p.
33 M. Kosmulski; *J. Colloid Interface Sci.*, **2009**, 337, 439-448.
34 B.B. Damaskin; "Electrochemistry", B.B. Damaskin, O.A. Petrii, G.A. Tsirlina; Koloss-Chemistry, Moscow, **2006**, 672 p.
35 G. Kh. Shabekova; "The current state of the theory of solvation and dissolution", G. Kh. Shabekova, L.I. Syzdykov; Kazak Universities, Almaty, **2004**, 352 p.
36 J. Schönherr, J. R. Buchheim, P. Scholz, P. Adelhelm; *J. of Carb. Research*, **2018**, 4, 21.